

Article

Polymeric Floating Photocatalysts Based on PE/TiO₂ Composites for the Removal of Organic Pollutants in Water

Valentina N. Panchenko, Mikhail A. Matsko *, Dmitry S. Selishchev  and Denis V. Kozlov

Borskov Institute of Catalysis SB RAS (BIC SB RAS), 630090 Novosibirsk, Russia; panchenko@catalysis.ru (V.N.P.)

* Correspondence: matsko@catalysis.ru

Abstract: Polymeric floating photocatalysts based on polyethylene (PE)/TiO₂ compositions were synthesized by in situ ethylene polymerization in the presence of a titanium–magnesium catalyst synthesized by the sequential deposition of a magnesium–aluminum complex and TiCl₄ on commercial TiO₂ P25. The optical band gap of the synthesized PE/TiO₂ composites was shown to be 3.1–3.3 eV, which allowed for their use as photocatalysts for the utilization of solar light. The photocatalytic activity of the PE/TiO₂ composites was studied for the degradation of methyl orange (MO) under irradiation with UV light ($\lambda_{\max} = 384$ nm). The composites containing 20–50 wt.% of PE were found to have an optimum combination between floatability and photocatalytic activity. The maximum photodegradation rate was observed at an MO concentration below 5 ppm. The polymeric PE/TiO₂ floating photocatalysts could be used repeatedly, but the long-term exposure of the composites to UV radiation was accompanied by oxidation of the polymer.

Keywords: polymeric floating photocatalysts; polymeric nanocomposites; methyl orange; photodegradation; TiO₂ Aeroxide Degussa P25



Citation: Panchenko, V.N.; Matsko, M.A.; Selishchev, D.S.; Kozlov, D.V. Polymeric Floating Photocatalysts Based on PE/TiO₂ Composites for the Removal of Organic Pollutants in Water. *J. Compos. Sci.* **2023**, *7*, 318. <https://doi.org/10.3390/jcs7080318>

Academic Editor: Francesco Tornabene

Received: 7 June 2023

Revised: 17 July 2023

Accepted: 25 July 2023

Published: 2 August 2023



Copyright: © 2023 by the authors. Licensee MDPI, Basel, Switzerland. This article is an open access article distributed under the terms and conditions of the Creative Commons Attribution (CC BY) license (<https://creativecommons.org/licenses/by/4.0/>).

1. Introduction

Dyes are widely used in the textile, paper, and food industries. A large amount of waste makes it necessary to develop efficient methods for their utilization. Photocatalytic degradation using solar light is a promising and environmentally friendly method for removing dyes from industrial wastewater. The development of photocatalysts for the efficient degradation of dyes under solar light is an important task.

Polymeric floating photocatalysts (FPCs), which consist of a floating matrix and TiO₂, ZnO, or other semiconductors, have been reported recently for the remediation of wastewater [1,2]. Various materials, namely, tree bark, perlite, vermiculite, and polymers, such as polyethylene (PE) and polythiophene (PTP), have been suggested for use as the floating matrix. These composites can improve semiconducting photocatalysts and enhance their efficiency. The anchoring of a photocatalyst on a floating substrate decreases its agglomeration, thus increasing the working surface of a catalyst. Floating photocatalysts are located at the water–air interface; therefore, maximum oxygenation can be reached due to the high power of solar radiation. In addition, FPCs do not require mixing, are reusable, and can easily be removed from the water surface after the remediation cycle. These features make it possible to employ FPCs in industrial sediment basins and reservoirs for contaminated wastewater, as well as for the removal of organic pollutants (oil and petrochemical spills) in the regions of natural water bodies enclosed with harbor booms. The most attractive substrates are polymers, particularly PE and PP. They are the most widespread materials; their easy recycling makes them relatively pure materials in ecological terms.

FPCs can be obtained by mixing the melt or solution of a polymer with a photocatalyst, for example, PE [3–5] and PP [6], or by the in situ polymerization of the corresponding monomer, for example, pyrrole [7,8] or thiophene [9]. Composite photocatalysts have been

found to be highly active in the photocatalytic degradation of dyes and exhibit antibacterial activity toward *Escherichia coli* [3,6].

The first two methods are quite simple and do not require special equipment. However, some features hinder their wide application, including the agglomeration of photocatalyst nanoparticles; the high temperatures required for obtaining the polymer melt, which often leads to polymer destruction; the limited solubility of polymers in many solvents; and the necessity to regenerate solvents. However, there are some publications on PP-nano-ZnO composites obtained by extrusion [6,10], mixing a cyclohexane solution of low-density PE with nano-TiO₂ [11], and mixing linear low-density PE (LLDPE) in a xylene solution with TiO₂ P25 [4].

The third method used to obtain composites—polymerization filling—is preferable. Three main approaches to the synthesis of such composites are known. The first approach involves the synthesis of a polymer in the presence of a photocatalyst. This technique was used, for example, to obtain polypyrrole/TiO₂ [8]; PE/TiO₂ and ethylene-octadecene/TiO₂ composites were synthesized in the presence of ethenyl(bisindenyl)zirconium dichloride (rac-EtInd₂ZrCl₂) as a catalyst and methylaluminoxane (MAO) [3]. The second approach is multistep: an active component (catalyst) is formed on the photocatalyst surface for further participation in polymer synthesis. This technique was employed to obtain TiO₂/polyacrylamide composites [12]. The third approach involves the simultaneous synthesis of a photocatalyst and a polymer. It was used to immobilize TiO₂ nanoparticles on mulberry wood flour [13].

Previously, we showed that PE/nano-Al₂O₃ and PE/Y₂O₃(Eu) composites can be obtained by using in situ ethylene polymerization [14,15]. To this end, a titanium–magnesium catalyst for ethylene polymerization was formed by the sequential deposition of a magnesium–aluminum complex (MAC) and TiCl₄ on a nano-Y₂O₃(Eu) surface. Such catalysts are highly active toward ethylene polymerization and allow the polymer molecular weight to vary across a wide range. In this study, a similar approach was applied to synthesize polymeric floating photocatalysts using a commercially available TiO₂ Aeroxide® P25.

The synthesized composites were studied in the photocatalytic degradation of methyl orange (MO). The effects of the MO concentration, the concentration of the composite, and the content of polymeric filler on the rate of MO degradation were investigated.

2. Materials and Methods

2.1. Reagents

A 0.84 M heptane solution of triethylaluminum (Al(C₂H₅)₃, TEA), TiCl₄, and a 0.5 heptane solution of dibutylmagnesium (Mg(C₄H₉)₂, MgBu₂) were purchased from Acros Organics (Geel, Belgium) and used for the catalytic polymerization of ethylene, as received without additional purification. Before use, the reagents were stored in an inert atmosphere. A commercially available TiO₂ Aeroxide P25 (TiO₂) from Evonik Ind. (Essen, Germany) was used as the photocatalytically active component. TiO₂ P25 had a rutile (20%) and anatase (80%) phase composition, a specific surface area of 56.3 m²/g, a crystal size of 30 nm, a pore volume of 0.42 cm³/g, and a bulk density of 0.150 g/cm³.

2.2. Synthesis of PE/TiO₂(P25) by In Situ Ethylene Polymerization

The synthesis of PE/TiO₂ composites was performed by in situ ethylene polymerization according to a previously published technique [14,15]. In the first step, the catalytic system TMC(P25) was prepared on the surface of a TiO₂ photocatalyst by sequential deposition of an organomagnesium compound, MgBu₂, and TiCl₄, onto TiO₂(P25). Before use, TiO₂ was dehydroxylated by calcination in air at 450 °C for 3 h, followed by treatment at the same temperature for another 3 h under vacuum. The final suspension of the polymerization catalyst was ultrasonicated for 30 min and then transferred to an autoclave for polymerization. The suspension polymerization of ethylene was carried out in a 0.7 L stainless steel autoclave at an ethylene pressure of 4 atm in the presence of TEA as a co-

catalyst (1.2 mmol/L) in heptane (250 mL). For some composites, hydrogen was introduced during polymerization at a pressure of 1 atm. The PE content in the PE/TiO₂ composites was controlled by varying the polymerization time.

The composites synthesized without hydrogen are referred to in the text as PE/TiO₂, whereas those formed in the presence of hydrogen are denoted as H-PE/TiO₂. All composites were stored in the dark to prevent oxidation of the polymer.

2.3. Characterization of Samples

2.3.1. TG Analysis of Composites

Thermal analysis of the samples was performed using an STA 449 C Jupiter simultaneous thermal analyzer (NETZSCH Group, Selb, Germany). The samples were placed in corundum crucibles for examination. Air was fed into a chamber with the sample at a rate of 30 mL/min. The sample was heated from room temperature to 30 °C at a rate of 2 °C/min. This was followed by temperature-programmed heating at a rate of 10 °C/min to 1000 °C. The experimental data were analyzed using the NETZSCH Proteus Thermal Analysis software package.

2.3.2. Scanning Electron Spectroscopy (SEM)

The SEM images of the PE/TiO₂ samples were obtained using a JSM 6460 LV scanning electron microscope (JEOL, Tokyo, Japan).

2.3.3. A DRIFTS Study

DRIFT spectra were taken on an FTIR-8400S instrument (Shimadzu, Kyoto, Japan) using a DRS-8400S attachment in the region of 400–6000 cm⁻¹ with a 4 cm⁻¹ step and accumulation over 100 scans. The spectra were expressed in absorption mode using the Kubelka–Munk function (Equation (1)):

$$F(R) = \frac{(1 - R)^2}{2 \cdot R} \quad (1)$$

where R is the reflectance

2.3.4. UV-Vis Spectroscopy

Powdered samples of TiO₂ and PE/TiO₂ were placed in a quartz cuvette ($l = 2$ mm) to measure the UV-vis diffuse reflectance spectra. The measurements were performed on a UV-2501 PC Shimadzu instrument using an IRS-250A diffuse reflectance attachment in the region of 190–900 nm with a step size of 2 nm. According to ref. [16], the optical bandgap (E_g) was estimated by approximating the Tauc plots using Equation (2):

$$F(R_\infty) h [\nu]^{1/2} = B (h\nu - E_g), \quad (2)$$

2.4. Photodegradation of MO

Methyl orange was dissolved in distilled water to prepare the MO solution with a concentration of 1–20 ppm. Photodegradation experiments were performed in a batch reactor containing 60 mL of the MO solution and 0.1 g of the PE/TiO₂ or n-PE/TiO₂ composite.

Before irradiation, the reaction mixture was kept in the dark for 1 h to establish the adsorption–desorption equilibrium of MO on the surface of the floating composite. After that, a UV lamp ($\lambda_{UV} \approx 384$ nm, 15 W) was switched on, and the reactor was exposed to UV light for 2–5 h. The UV lamp was placed on top at a distance of 10 cm from the surface of the solution. The experiments were carried out without stirring the MO solution (as a model of a floating photocatalyst in the environment).

After the first run, the composite was washed with deionized water and dried for further reuse.

To investigate the kinetics of MO adsorption and photodegradation, a probe for analysis using UV-vis spectroscopy was sampled from the reaction mixture every 15–30 min. UV-vis

spectra were measured on a UV-2501 PC Shimadzu instrument using a quartz cuvette ($l = 10$ mm).

Kinetic plots of MO adsorption and degradation were calculated using Equation (3) based on the optical density at 464 nm, which was attributed to the characteristic absorption of MO:

$$\eta = (1 - D/D_0) \times 100\% \quad (3)$$

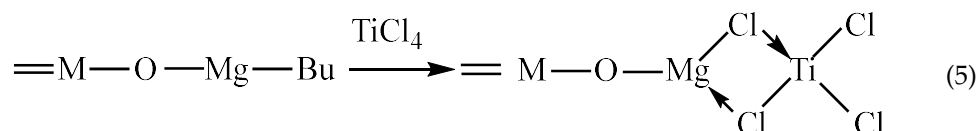
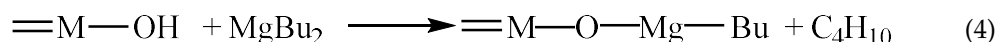
where D_0 is the initial optical density of the MO solution and D is the optical density of the solution measured during the reaction.

3. Results

3.1. Synthesis of the PE/TiO₂ Material

The PE/TiO₂ composites were synthesized using TiO₂ P25, which consisted of 80 wt.% anatase and 20 wt.% rutile. In the first step, the catalytic system TMC(P25) was prepared on the surface of a TiO₂ photocatalyst by the sequential deposition of an organomagnesium compound, MgBu₂, and TiCl₄, onto TiO₂(P25), which was preliminarily dehydroxylated at 450 °C. In the second step, ethylene polymerization was performed.

Our earlier study, in which IR spectroscopy was used [16], revealed that the sequential deposition of MAC and TiCl₄ on aluminum nano-oxide Nafen results in the formation of a titanium–magnesium active component with a composition close to that of known titanium–magnesium catalysts (TMCs) containing TiCl₃ and MgCl₂. The main reaction is the interaction of MgBu₂ with the OH groups of Al₂O₃ (reaction (4)), leading to the anchoring of the organomagnesium compound on the surface of the aluminum nano-oxide Nafen, and the subsequent interaction of TiCl₄ with surface organomagnesium groups (reaction (5)). This interaction was accompanied by the reduction in TiCl₄ and the formation of a catalyst containing magnesium oxychloride and titanium trichloride, which were anchored on the aluminum oxide surface.

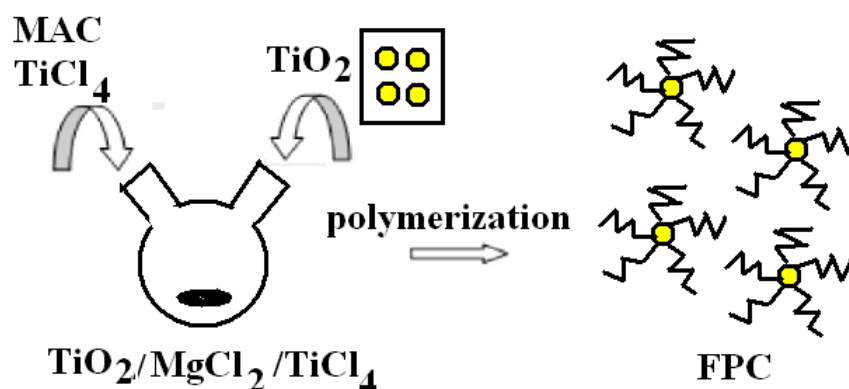


Presumably, similar reactions occurred on the TiO₂ surface during the sequential deposition of MAC and TiCl₄.

Under polymerization conditions, the interaction of compound (A) with the TEA co-catalyst results in the formation of active sites containing alkylated Ti³⁺ compounds, which are involved in ethylene polymerization and lead to the formation of PE on the TiO₂ surface.

Chemical analysis data showed that TMC(P25) contains 1.13 wt.% of Mg. According to ref. [16], MAC interacts predominantly with isolated μ_1 -OH groups. Under the assumption of the specific interaction of MAC with the μ_1 -OH groups of titanium oxide, their amount in TiO₂ was 765 $\mu\text{mol/g}$.

It is known [17] that TiO₂ nanoparticles tend to form agglomerates and associates due to their high surface energies. To ensure a uniform distribution of TiO₂ in the polymer matrix, enhance the dispersion stability of TiO₂ nanoparticles, and create interfaces between the organic and inorganic phases, the surface of the filler is commonly modified with alkoxy silanes, fluoro-silane, and glycidyl methacrylate. Presumably, the anchoring of TMC on the surface of the TiO₂ photocatalyst also decreases the agglomeration of nanoparticles. However, this effect was observed during the polymer synthesis (Scheme 1). Indeed, our TEM study [15] demonstrated that Y₂O₃(Eu) filler particles were uniformly distributed in PE/Y₂O₃(Eu) composites.



Scheme 1. Scheme of the synthesis of a floating PE/TiO₂ photocatalyst.

3.2. Characterization of FPCs

Figure 1 shows the SEM images of TiO₂ and two H-PE/TiO₂ composites obtained by TMC(P25), with 28.5 and 85.4 wt.% PE content, respectively. The initial TiO₂ consisted of fine spherical particles with a diameter smaller than 50 nm (according to the XRD data, the average size of the TiO₂ crystallites was 30 nm). The H-PE/TiO₂ composites also consisted of spherical particles, but they were larger in size. The diameter of the particles increased with increasing PE content (Figure 1b,c). The SEM data suggest that PE was formed around the TiO₂ crystallites (Scheme 1).

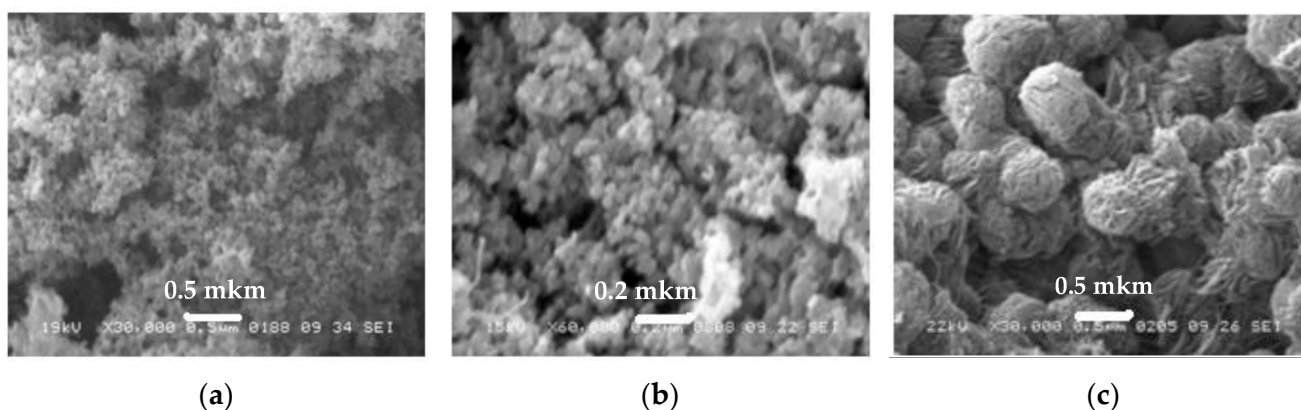


Figure 1. SEM images of (a) TiO₂, (b) H-28.5PE/TiO₂, (c) and H-85.4PE/TiO₂.

The PE content in the synthesized PE/TiO₂ composites was estimated from the polymer yield, measured as the difference between the masses before and after polymerization (Table 1). The thermogravimetric differential thermal analysis (TG-DTA) was used for the analysis of the PE content. Figure 2 shows the TG curves for the PE/TiO₂ and H-PE/TiO₂ composites, in which the estimated content of the polymer was 38.2 and 40.5 wt.%, respectively. Three regions could be distinguished in the TG curves from the studied samples. The first region, at 30–200 °C, corresponded to the removal of physically adsorbed water. The second region, at 200–500 °C, was related to the degradation of the polymer in the composite [18]. The third region, at 500–1000 °C, was the phase transformation of anatase to rutile. The n-PE/TiO₂ composite, which was obtained by polymerization in the absence of hydrogen and hence contains higher molecular weight PE, decomposed at a higher temperature compared to the H-PE/TiO₂ sample (Figure 2).

According to the TG-DTA data, the total weight losses in the PE/TiO₂ and H-PE/TiO₂ samples were 34.8 and 39.3 wt.%, which corresponded to the PE content of 29.6 and 34.4 wt.%, respectively. These data were close to the polymer content measured by the gravimetric method (Table 1). A slight difference between the data of gravimetry and TG-TGA analysis was because the result of the gravimetric method included the weight of

physically adsorbed water. Further in the text, the polymer content measured using the gravimetric method is indicated.

Table 1. Weight change of the H-PE/TiO₂ and PE/TiO₂ composites according to TG-DTA analysis.

Sample	Changing Weight at Definite Temperatures, % wt.				Total Changing Weight % wt.	Content of PE, % wt.	
	100–160 °C	200–290 °C	290–400 °C	400–500 °C	TG-TGA	TG-TGA	For yield of PE
PE/TiO ₂	5.2	2.2	15.7	11.7	34.8	29.6	38.2
H-PE/TiO ₂	4.9	2.7	18.3	13.4	39.3	34.4	42.8

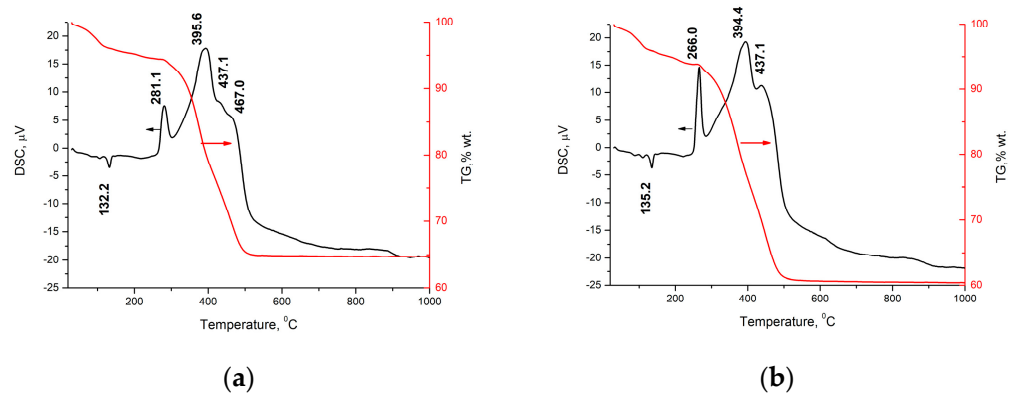


Figure 2. DSC and TG curves for (a) 38.2PE/TiO₂ and (b) H-40.5PE/TiO₂ composites.

The main characteristic of a photocatalyst is the band gap (E_g). Figure 3 shows the electronic spectra of TiO₂ and the two PE/TiO₂ composites with PE content of 26.1 and 60.0 wt.%. Figure 4 shows the electronic spectra of TiO₂ and two H-PE/TiO₂ composites with PE content of 55.8 and 85.4 wt.%. Equation (2) was used to fit the Tauc plots and calculate the bandgap (E_g). The initial TiO₂ photocatalyst had a gap E_g of 3.0 eV. The gap E_g calculated for the TiO₂ sample coincided with the literature data for rutile [19]. Coating the TiO₂ photocatalyst with the polymer led to an increase in E_g . With an increasing PE content, E_g gradually increased. For the 26.1PE/TiO₂ and 60PE/TiO₂ samples, E_g was equal to 3.2 and 3.3 eV, whereas, for the H-55.8PE/TiO₂ and H-85.4PE/TiO₂ samples, it was 3.1 and 3.2 eV, respectively. According to ref. [18], LDPE has an optical energy gap between the valence band and the conduction band (E_g^{opt}) of 3.1–3.6 eV. Thus, the increase in E_g in the PE/TiO₂ and H-PE/TiO₂ composites can be attributed to an increase in the PE layer thickness in the samples under consideration.

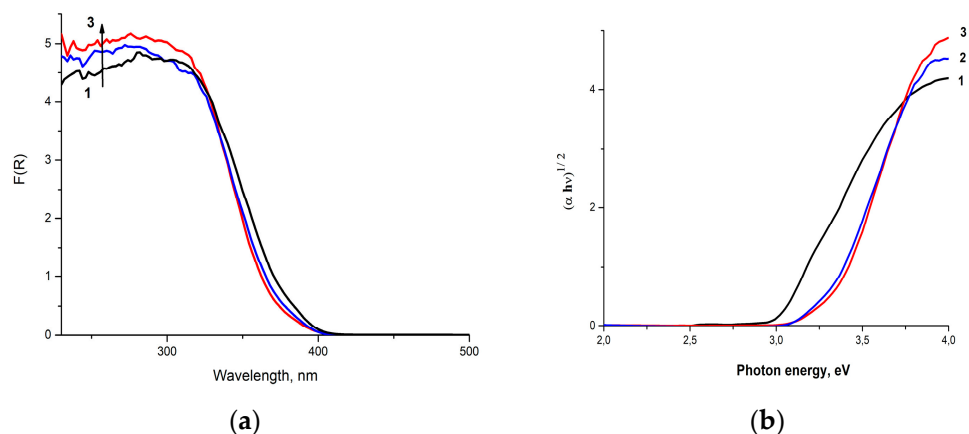


Figure 3. Kubelka–Munk (a) and Tauc (b) plots for (1) TiO₂, (2) 26.1PE/TiO₂, and (3) 60.0PE/TiO₂ samples.

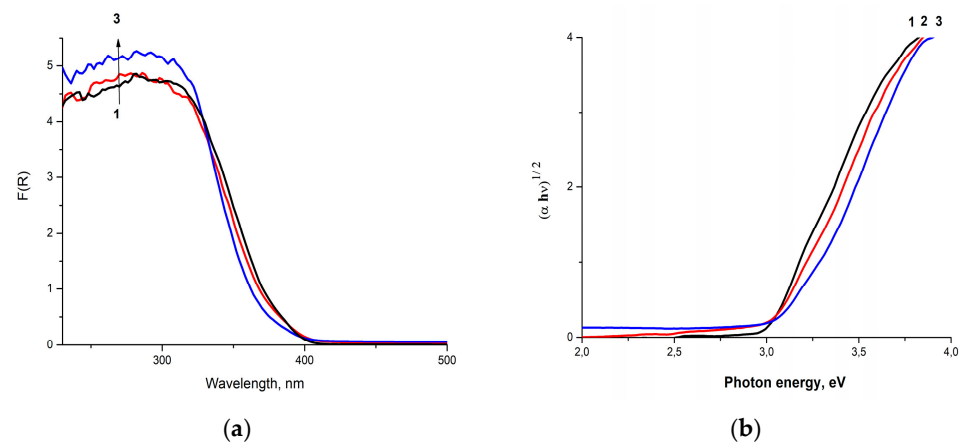


Figure 4. Kubelka–Munk (a) and Tauc (b) plots for (1) TiO_2 , (2) H-55.8PE/ TiO_2 , and (3) H-85.4PE/ TiO_2 samples.

Mixing TiO_2 with water leads to the formation of a suspension, which rapidly segregates (Figure 5a,b). Upon the addition of H-17.5PE/ TiO_2 powder to water, only 1–3 wt.% of the sample settles down. The PE/ TiO_2 and H-PE/ TiO_2 samples that contain more than 20 wt.% of PE sit in the water well and do not sink for a long time (Figure 5c,d). These results show that the PE content in the PE/ TiO_2 composites determines their floatability.

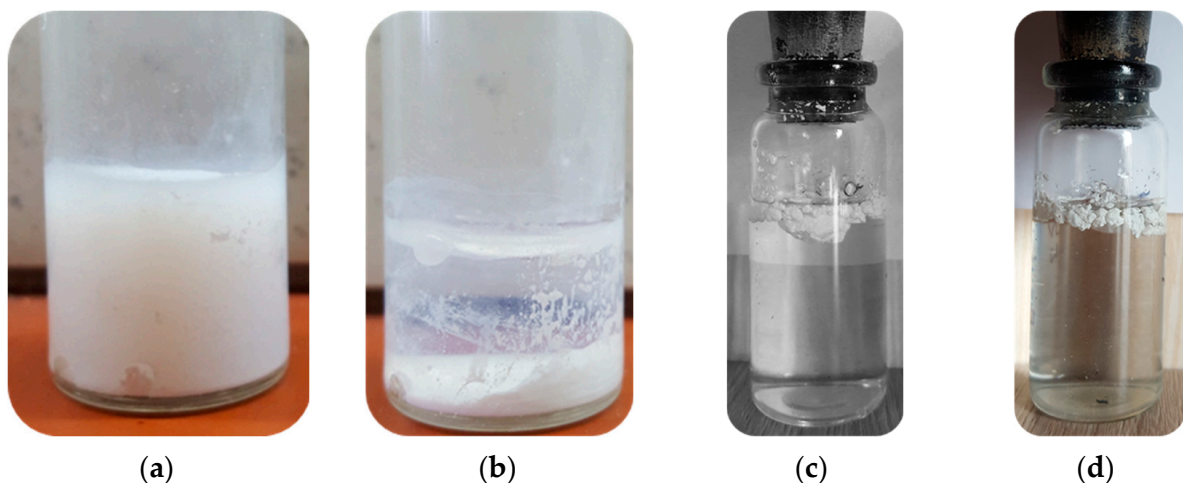


Figure 5. Photographs of TiO_2 (a) suspended in water and (b) stored for 24 h; (c) polymeric H-28.5PE/ TiO_2 composite added to water and (d) stored for 30 days.

3.3. PECs Performance in Photocatalytic Degradation of Methyl Orange

To study the properties of photocatalysts for the decomposition of organic substances, simple model compounds were employed [20–31]. We used methyl orange (MO), which is one of the most studied compounds. This made it possible to compare the performance of the new photocatalysts with those already known.

3.3.1. Correlation between Adsorption and Degradation of MO

It is known [1,2] that the amount of adsorbed dye is an important parameter affecting its photodegradation rate. Figure 6 illustrates the kinetics of MO adsorption onto the 26.1PE/ TiO_2 and H-28.5PE/ TiO_2 composites. One can see that the adsorption–desorption equilibrium in the system was established in 6 h. A possible reason for this is that water is a non-wetting liquid for PE, and the study was performed without stirring the mixture.

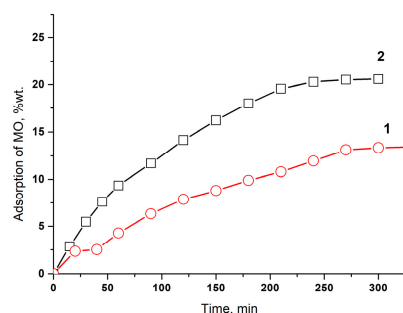


Figure 6. Kinetic plots of MO adsorption ($C_{MO} = 5$ ppm, $pH = 6.7$) on the surface of (1) 26.1PE/TiO₂; (2) H-28.5PE/TiO₂.

It should be noted that the amount of dye adsorbed by the 26.1PE/TiO₂ composite, which was obtained without hydrogen, was two times smaller than that adsorbed by H-28.5PE/TiO₂.

Figure 7 illustrates the change in the concentration of MO under UV irradiation in the absence and presence of the PE/TiO₂ composite, as well as the adsorption of MO in the presence of the composite. It can be seen that MO decomposition practically did not occur in the absence of the catalyst (Figure 7a, curve 1). In the presence of PE/TiO₂, the adsorption of MO was observed (Figure 7a, curve 2). When the UV irradiation was turned on in the presence of the PE/TiO₂ composite, the decomposition of MO increased significantly (Figure 7a, curve 3 and Figure 7b).

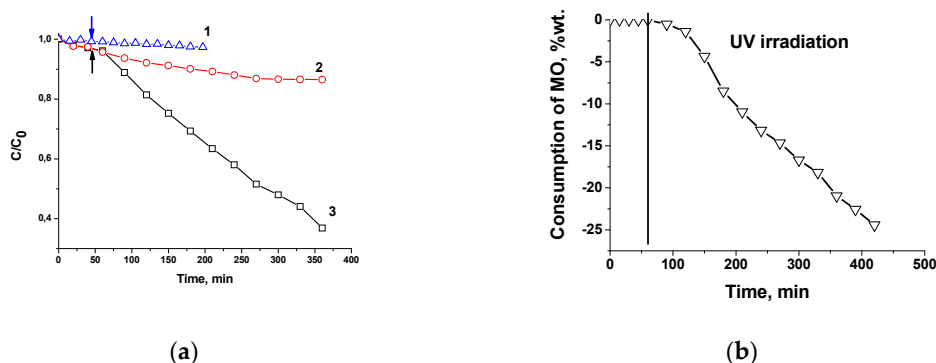


Figure 7. (a) Changes in the concentration of MO ($C_{MO} = 5$ ppm, $pH = 6.7$). (1) UV irradiation without the addition of PE/TiO₂; (2) adsorption of MO in the presence of 26.1 PE/TiO₂; (3) UV irradiation in the presence of 26.1 PE/TiO₂; (a) UV radiation; (b) degradation of MO: curve (2) subtracted from curve (3).

3.3.2. Effect of the Polymer Content in the PE/TiO₂ Composite on Catalyst Performance

Figure 8 shows the kinetics of MO photodegradation over the H-PE/TiO₂ composites containing 17.5, 42.8, 55.8, and 85.4 wt.% of PE. Table 2 lists the amounts of MO adsorbed in 1 h and decomposed after 4 h of exposure to UV radiation. It can be seen that the amounts of adsorbed MO and decomposed MO (C_{MO}) decreased with increasing polymer content in the composite (Table 2), which may be related to an increase in the accessibility of TiO₂ with a decrease in the thickness of the polymer layer.

The linear dependence of $\ln(C/C_0)$ -t shows that the degradation of MO follows a pseudo-first-order (Figure 8b).

Note that in the presence of the H-17.5PE/TiO₂ composite, cloudiness of the MO solution is observed after 2.5 h of exposure to UV radiation, and after 5 h, the composite settles down. This may be due to the partial degradation of the polymer under UV radiation. Indeed, it is known [20,30–32] that the irradiation of PE with UV or solar light leads to its oxidation. This issue is discussed in detail below.

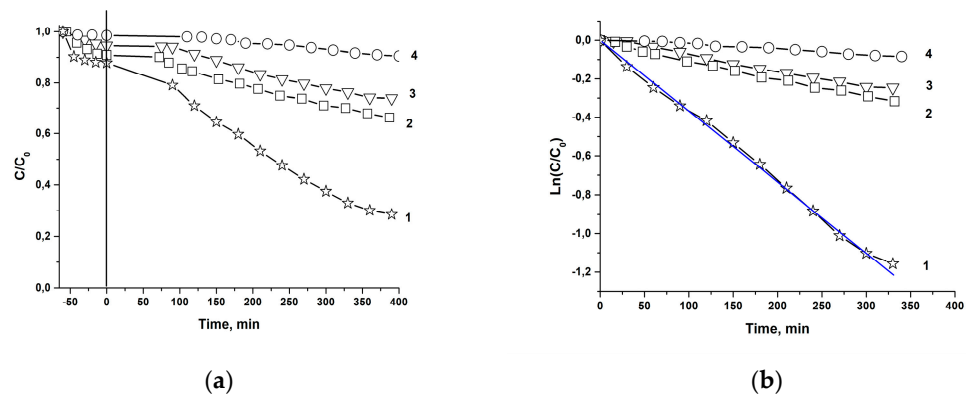


Figure 8. Effect of PE content in the H-PE/TiO₂ composites on the rate of MO photodegradation: (a) linear scale and (b) logarithmic scale. (1) 17.5 wt.%, (2) 42.8 wt.%, (3) 55.8 wt.%, and (4) 85.4 wt.%.

Table 2. Effect of PE content in the H-PE/TiO₂ composites on the discoloration of MO.

Sample	PE, wt%	MO ppm	pH ₀	pH _e	Changing of MO %	
					for 1 h Adsorption	for 4 h UV-Radiation
1	17.5	5	6.7	5.4	12.1	55.5
2	42.8	5	6.9	5.4	9.2	33.0
3	55.8	5	6.9	5.8	5.5	22.4
4	85.4	5	6.7	6.6	1.3	0.5

In the presence of the H-42.8PE/TiO₂ and H-55.85PE/TiO₂ composites, the C_{MO} is not high and constitutes 33.0 and 22.4 wt.%, respectively (Table 2, expts. 2 and 3). Nevertheless, these values are comparable with the data reported in ref. [20], which was devoted to the photodegradation of methylene blue, indigo carmine, and drimaren red under the action of UV (Hg, 254 nm) or solar irradiation in the presence of a floating photocatalyst based on TiO₂ P25 grafted on expanded polystyrene (EPS) with a TiO₂ content of 1, 7, and 18 wt.%. The maximum activity (40–55% degradation at an FPC loading of 1 g) was observed for 18%TiO₂/EPS.

It is known [22–24] that the photodegradation of MO is a complicated multistep process. The final products of photodegradation are carbon dioxide and aliphatic acids. This means that, at the end of the MO photodegradation, the acidity of the medium should change. Indeed, the pH of the MO solution decreases at the end of the reaction from pH₀ = 6.7–6.9 to pH_e = 5.4–5.8 (Table 2).

3.3.3. Effect of the MO Concentration

Figure S2 and Table 3 (exps. 1, 2, 5, and 6) list the amounts of MO adsorbed in 1 h in the dark. One can see that a decrease in the MO concentration was accompanied by an increase in the amount of adsorbed MO.

The results obtained were consistent with the data reported in ref. [25], which demonstrated that the adsorption equilibrium for the PTP/TiO₂ composites depends on the MO concentration. At MO concentrations of 1 and 10 ppm, the adsorption ratio of the MO solution was equal to 28 and 8%, respectively.

The amount of MO that decomposed during 4 h of exposure to UV radiation in the presence of the 26.1PE/TiO₂ composite also depended on the concentration of the MO solution. One can see that a decrease in the MO concentration led to an increase in C_{MO}.

Our results agree with the data reported for TiO₂ [26–28] and PTP/TiO₂ composites [30]. In these studies, the maximum rate of MO photodegradation for all the photocatalysts was observed at concentrations below 5 ppm (1.6 mM). This effect was attributed to

the blocking of those active sites on the photocatalyst surface, which were involved in the formation of radicals. This effect could also be the main cause of the deterioration of the degradation activity in the presence of the 26.1PE/TiO₂ composite.

Table 3. Effect of the concentration of MO on pH, and degradation of MO in the presence 26.1PE/TiO₂ composite.

Sample	Concentration of MO, ppm	S _{BET} , m ² /g	pH ₀	pH _e	Changing of MO %	
					for 1 h Adsorption	for 4 h UV-Radiation
1	1.7	-	6.7	6.4	8.4	16.7
2	5.0	32.6	6.7	6.4	4.5	12.5
3 ¹	5.0	36.3	6.7	6.4	4.3	12.8
4 ²	5.0	45.2	6.7	6.6	4.3	38.9
5	15.0	-	6.9	6.9	4.0	5.5
6	20.0	-	6.9	6.9	4.0	2.0

¹ 2 cycles, ² 3 cycles.

3.3.4. Effect of the PE/TiO₂ Composite Concentration

Table 4 lists the dependence of C_{MO} on the loading of the 38.2PE/TiO₂ and H-40.5PE/TiO₂ composites. One can see that the composite loading changes symbiotically with the amount of decomposed MO. An increase in the loading of 38.2PE/TiO₂ and H-40.5PE/TiO₂ from 0.1 g to 0.5 g leads to an increase in C_{MO} from 12.5% to 77.7 wt.% and from 9.0% to 68.8 wt.%, respectively. C_{MO} normalized to the FPC weight also changes for 38.2PE/TiO₂ and H-40.5PE/TiO₂ from 12.5% to 15.5% and from 9.0% to 13.8%, respectively.

Table 4. Effect of the load of 38.2PE/TiO₂ and H-40.5PE/TiO₂ composites on pH, and the degradation of MO.

Sample	C(MO), ppm	Load of FPC, g	pH ₀	pH _e	Changing of MO for 4 h UV Radiation, %wt.	
					Total	for Load of Catalyst
38.2PE/TiO ₂						
1	5	0.1	6.7	6.4	12.5	12.5
2	5	0.2	6.7	6.4	24.0	12.0
3	5	0.5	6.7	4.0	77.7	15.5
H-40.5PE/TiO ₂						
4	5	0.1	7.2	6.1	9.0	9.0
5	5	0.5	6.7	5.7	68.8	13.8

It is known [21,33,34] that the amount of photocatalyst is an essential parameter determining the photodegradation rate of dyes because it determines the number of active surface sites involved in the formation of OH radicals. At the same time, ref. [21] studied the photodegradation of dyes in the presence of a floating photocatalyst based on TiO₂ P25 grafted on expanded polystyrene (EPS), and it was noted that the degradation rate nonlinearly depends on the photocatalyst concentration. At certain concentrations (depending on the catalyst type), the rate plateaued. This result could be related to the effect of oxygenation; dye diffusion may also control the reaction rate. For TiO₂, which is not a floating photocatalyst, its high concentration can lead to a decrease in the photodegradation rate, which is caused by the blocking of UV radiation due to the formation of a cloudy suspension [33,34].

Figure 9 illustrates the changes in the UV-vis spectra of MO solutions during the adsorption and photodegradation with loaded 0.5 g of the 38.2PE/TiO₂ and H-40.5PE/TiO₂ composites. It is seen that the changes in the UV-vis spectra depend on the polymer structure.

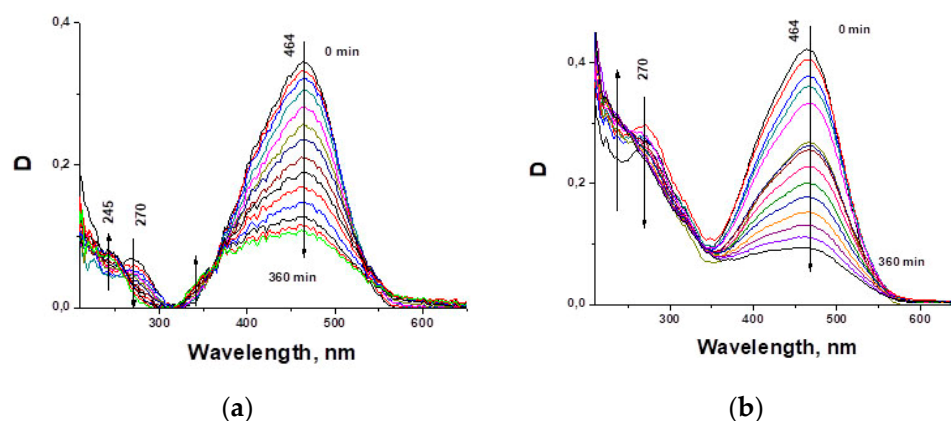


Figure 9. Changes in UV-vis spectra of a reaction solution during adsorption and degradation of MO over (a) H-40.5PE/TiO₂ and (b) 38.2PE/TiO₂.

During the MO degradation in the presence of the 38.2PE/TiO₂ composite, the intensities of the bands at 270 and 464 nm decrease, which testifies to the adsorption of MO, and the intensity of the absorption band in the region of 210–300 nm increases, which indicates the appearance of MO degradation products.

When the H-40.5PE/TiO₂ composite is used as a photocatalyst, photodegradation is also accompanied by a decrease in the intensity of the absorption bands at 270 and 464 nm. At the same time, new bands appear in the regions of 210–300, 300–400, and 550–700 nm, the intensity of which increases with time. The appearance of these bands indicates that the MO degradation products pass into the solution. This may be related to the structural characteristics of the polymers in the 38.2PE/TiO₂ and H-40.5PE/TiO₂ composites. In the case of the polymer obtained without hydrogen, the molecular weight of the polymeric part is higher and diffusion limitations may occur.

3.3.5. Re-Use of PE/TiO₂ Composites

The possibility to reuse FPCs is also one of the important characteristics of photocatalysis. Table 3 (exps. 2–4) lists the changes in the MO amount after three cycles in the presence of the n-26.1PE/TiO₂ composite. One can see that C_{MO} in the first two cycles is close and equal to 12.5 and 12.8 wt.% (Table 3, exps. 2,3). After the third cycle, C_{MO} sharply increases to 38.9 wt.% (Table 3, exp. 4).

It is known [7,30–32] that exposure to UV or solar light leads to the oxidation of PE, which may result in its degradation. This suggests that UV radiation is accompanied by both the degradation of the basic MO dye and the decomposition of the polymeric substrate. To verify this hypothesis, we measured the surface area of the 26.1PE/TiO₂ composite after each cycle (Table 3). It is seen that after each cycle, the surface area increases (32.6, 36.3, and 45.2 m²/g) and approaches that of the initial TiO₂ (56.3 m²/g). An increase in the S_{BET} may testify to the appearance of pores in the composite.

Figure 10 shows the DRIFT spectra in the vibrational region of the carbonyl groups for the initial composite 26.1PE/TiO₂ and after the third cycle. A broad absorption band with a maximum of 1640 cm⁻¹ (δ of the OH groups of adsorbed water) is observed in the spectrum of the composite in the region of 1500–1800 cm⁻¹ (Figure 9, spectrum 1). After the third cycle, the band in this region broadens (Figure 9, spectrum 2). The deconvolution of the spectrum made it possible to distinguish the bands at 1590, 1640, and 1695 cm⁻¹. The appearance of bands at 1590 and 1695 cm⁻¹ indicates the formation of ketone, carbonyl, and carboxyl groups [35]. Thus, the data obtained demonstrate that UV irradiation is accompanied not only by the degradation of MO but also by the oxidation of the polymer matrix.

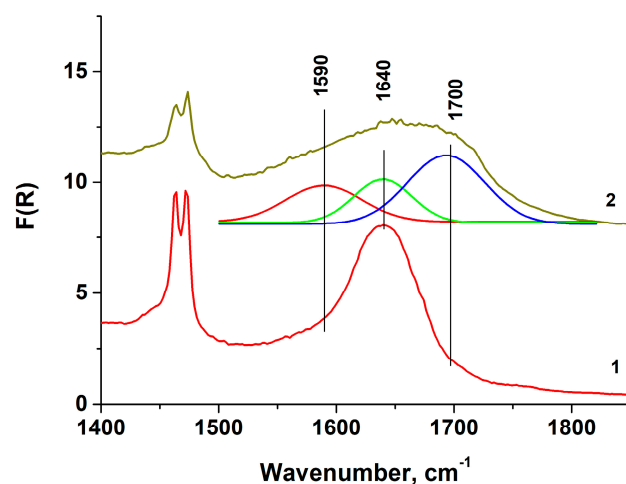


Figure 10. DRIFT spectra of 26.1PE/TiO₂ composite before (1) and after 3 cycle (2).

4. Conclusions

For the first time, floating PE/TiO₂ photocatalysts with a polymer content of 17.5–85.4 wt.% were synthesized by the in situ polymerization method using TMC(P25) as a polymerization catalyst. TMC(P25) was synthesized by sequential deposition of the organomagnesium compound, MgBu₂, and TiCl₄ on the surface of a TiO₂ photocatalyst and was used for ethylene polymerization in suspension.

The SEM study revealed that the particles of the initial TiO₂ photocatalyst and those of the composites had a similar spherical shape but different sizes. The diameters of the particles in the composites depended on the content of the polymer. For example, at PE contents of 28.5 and 85.4%, the diameters of the particles were 80–100 and 150–200 nm, respectively. The polymer replication effect suggests that the filler (TiO₂ photocatalyst) was uniformly distributed in the polymer matrix.

One of the main characteristics of photocatalysts is the band gap (E_g). The gap E_g of the PE/TiO₂ composites was equal to 3.1–3.3 eV, which allowed their application as photocatalysts for the utilization of solar light. Under UV radiation ($\lambda_{\max} = 384$ nm), the synthesized composites decomposed the MO. As the MO concentration increased, the efficiency of photocatalytic degradation decreased, which was primarily related to the blocking of the sites for the formation of OH radicals. The maximum photodegradation rate was observed at MO concentrations below 5 ppm.

The content of the polymer matrix in the composite affects its floatability and MO photodegradation rate. The best characteristics were obtained for the composites containing 20–50 wt.% of PE. This was primarily associated with the accessibility of MO to the surface of the TiO₂ photocatalyst because the polymer was formed around the TiO₂ particle; thus, an increase in the PE content in the composite led to an increase in the thickness of the polymer matrix (Scheme 1).

The efficiency of photodegradation also depended on the amount of the applied PE/TiO₂ composite. When the loading of the 38.2PE/TiO₂ and H-40.5PE/TiO₂ composites increased from 0.1 to 0.5 g, C_{MO} increased from 12.5 to 77.7 wt.% and from 9 to 68.8 wt.%, respectively.

The composites could be reused at least three times. However, the process of decomposition of the polymer matrix is clearly observed (TiO₂ gradually decomposed the polymer under UV radiation). These are the main advantages of floating photocatalysts. After the removal of organic pollutants from the environment, the PE layer is likely to be decomposed completely by UV radiation and the only byproduct is an inert TiO₂.

5. Concluding Remarks and Further Work

The first results of the use of PE/TiO₂ composites obtained by in situ polymerization for the decomposition of organic waste (for example, MO) allowed us to identify a number

of important correlations that are necessary to continue the work. First, it is necessary to test this method for the decomposition of hydrocarbons (oil wastes are the most probable). Second, it is necessary to choose the optimal content of the polymer part. On the one hand, the polymer part is necessary for the floating ability of the photocatalyst; on the other hand, the loss of TiO₂ activity due to its complete encapsulation by the polymer layer should be avoided. It is also necessary to optimize the morphology (porosity) and structure of the polymer matrix (for example, by obtaining copolymers of ethylene with hexene-1 or propylene) to accelerate the self-decomposition of the polymer part of the composites after the removal of organic waste from the water surface. Third, it seems promising to continue the search for a more active form of TiO₂ to improve catalyst performance.

Supplementary Materials: The following supporting information can be downloaded at: <https://www.mdpi.com/article/10.3390/jcs7080318/s1>, Figure S1: (A) Changes in the concentration of MO (CMO = 5 ppm, pH = 6.7): (1) UV irradiation without composite, (2) adsorption of MO in the presence of 26.1PE/TiO₂, and (3) UV irradiation in the presence of 26.1PE/TiO₂ ((A) UV radiation and (B) degradation of MO: the difference between curve (3) and curve (2)); Figure S2: Effect of concentration of MO on the discoloration of MO dye in the presence of 26.1PE/TiO₂: Concentration of MO (1) 1.7 ppm, (2) 5 ppm, and (3) 15 ppm; Figure S3: UV-vis spectra of MO during adsorption and the discoloration in the presence of 26.1PE/TiO₂: (A) 1 cycle, (B) 3 cycles.

Author Contributions: Conceptualization, V.N.P., D.V.K. and M.A.M.; methodology, V.N.P.; validation, V.N.P., D.S.S. and M.A.M.; formal analysis, M.A.M. and V.N.P.; investigation V.N.P. writing—original draft preparation, V.N.P. and D.S.S.; writing—review and editing, D.V.K. and M.A.M.; supervision, D.V.K. and M.A.M.; project administration, D.V.K. and M.A.M. All authors have read and agreed to the published version of the manuscript.

Funding: This research was funded by the Ministry of Science and Higher Education of the Russian Federation (project AAAA21-121011490008-3).

Data Availability Statement: Data are contained within the paper and Supplementary Materials.

Acknowledgments: The authors thank V.A. Zakharov for some important notes.

Conflicts of Interest: The authors declare no conflict of interest.

References

1. Nasir, A.M.; Jaafar, J.; Aziz, F.; Yusof, N.; Salleh, W.N.W.; Ismail, A.F.; Aziz, M. A review on floating nanocomposite photocatalyst: Fabrication and applications for wastewater treatment. *J. Water Process Eng.* **2020**, *36*, 101300. [[CrossRef](#)]
2. Sacco, O.; Venditto, V.; Pragliola, S.; Vaiano, V. Composite Systems Based on N-Doped TiO₂/Polymeric Materials for Visible-Light-Driven Pollutant Degradation: A Mini Review. *Photochem* **2021**, *1*, 330–344. [[CrossRef](#)]
3. Yañez, D.; Guerrero, S.; Lieberwirth, I.; Ulloa, M.T.; Gomez, T.; Rabagliati, F.M.; Zapata, P.A. Photocatalytic inhibition of bacteria by TiO₂ nanotubes-doped polyethylene composites. *Appl. Catal. A Gen.* **2015**, *489*, 255–261. [[CrossRef](#)]
4. Magalhães, F.; Moura, F.C.C.; Lago, R.M. TiO₂/LDPE composites: A new floating photocatalyst for solar degradation of organic contaminants. *Desalination* **2011**, *276*, 266–271. [[CrossRef](#)]
5. Romero-Sáez, M.; Jaramillo, L.Y.; Saravanan, R.; Benito, N.; Pabón, E.; Mosquera, E.; Gracia, F. Notable photocatalytic activity of TiO₂-polyethylene nanocomposites for visible light degradation of organic pollutants. *Express Polym. Lett.* **2017**, *11*, 899–909. [[CrossRef](#)]
6. Prasert, A.; Sontikaew, S.; Sriprapai, D.; Chuangchote, S. Polypropylene/ZnO Nanocomposites: Mechanical Properties, Photocatalytic Dye Degradation, and Antibacterial Property. *Materials* **2020**, *13*, 914. [[CrossRef](#)]
7. Li, S.; Xu, S.; He, L.; Xu, F.; Wang, Y.; Zhang, L. Photocatalytic Degradation of Polyethylene Plastic with Polypyrrole/TiO₂ Nanocomposite as Photocatalyst. *Polym.-Plast. Technol. Eng.* **2010**, *49*, 400–406. [[CrossRef](#)]
8. Wang, D.; Wang, Y.; Li, X.; Luo, Q.; An, J.; Yue, J. Sunlight photocatalytic activity of polypyrrole–TiO₂ nanocomposites prepared by ‘in situ’ method. *Catal. Commun.* **2008**, *9*, 1162–1166. [[CrossRef](#)]
9. Bassaid, S.; Benhaoua, C.; Taleb, M.; Sahli, M.; Dehbi, A. Physical and Chemical Properties of Composites Based on Polythiophene and Titanium Dioxide Nanoparticles for Photocatalysis. *Polym. Sci. Ser. B* **2021**, *63*, 291–303. [[CrossRef](#)]
10. Xing, Z.; Zhang, J.; Cui, J.; Yin, J.; Zhao, T.; Kuang, J.; Xiu, Z.; Wan, N.; Zhou, W. Recent advances in floating TiO₂-based photocatalysts for environmental application. *Appl. Catal. B Environ.* **2018**, *225*, 452–467. [[CrossRef](#)]
11. Thomas, R.T.; Nair, V.; Sandhyarani, N. TiO₂ nanoparticle assisted solid phase photocatalytic degradation of polythene film: A mechanistic investigation. *Colloids Surf. A Physicochem. Eng. Asp.* **2013**, *422*, 1–9. [[CrossRef](#)]

12. Tang, Q.; Lin, J.; Wu, Z.; Wu, J.; Huang, M.; Yang, Y. Preparation and photocatalytic degradability of TiO₂/polyacrylamide composite. *Eur. Polym. J.* **2007**, *43*, 2214–2220. [[CrossRef](#)]
13. Ye, J.; Chao, C.; Hong, J. Preparation of a novel nano-TiO₂ photocatalytic composite using insoluble wood flour as bio-carrier and dissolved components as accelerant. *J. Mater. Res. Technol.* **2020**, *9*, 11255–11262. [[CrossRef](#)]
14. Panchenko, V.N.; Zakharov, V.A.; Matsko, M.A. Study of the Bis(imino)pyridyl Complex of Fe(II)/Nafen and Titanium-Magnesium/Nafen Catalysts for Synthesis of Polyethylene/Nafen Composites by in situ Ethylene Polymerization. *Polym. Sci. Ser. B* **2022**, *64*, 393–401. [[CrossRef](#)]
15. Kostyukov, A.I.; Panchenko, V.N.; Rakhmanova, M.I.; Nashivochnikov, A.A.; Matsko, M.A.; Suprun, E.A. Optical properties of composites based on polyethylene and monoclinic Y₂O₃:Eu³⁺ nanoparticles. *Mater. Chem. Phys.* **2021**, *273*, 125140. [[CrossRef](#)]
16. Wojciech, M. How To Correctly Determine the Band Gap Energy of Modified Semiconductor Photocatalysts Based on UV–Vis Spectra. *J. Phys. Chem. Lett.* **2018**, *9*, 6814–6817. [[CrossRef](#)]
17. Cazan, C.; Enesca, A.; Andronic, L. Synergic Effect of TiO₂ Filler on the Mechanical Properties of Polymer Nanocomposites. *Polymers* **2021**, *13*, 2017. [[CrossRef](#)]
18. Madani, M. Structure, optical and thermal decomposition characters of LDPE graft copolymers synthesized by gamma irradiation. *Curr. Appl. Phys.* **2011**, *11*, 70–76. [[CrossRef](#)]
19. Lan, Y.; Lu, Y.; Ren, Z. Mini review on photocatalysis of titanium dioxide nanoparticles and their solar applications. *Nano Energy* **2013**, *2*, 1031–1045. [[CrossRef](#)]
20. Babu, B.; Mallikarjuna, K.; Venkata Reddy, C.; Park, J. Facile synthesis of Cu@TiO₂ core shell nanowires for efficient photocatalysis. *Mater. Lett.* **2016**, *176*, 265–269. [[CrossRef](#)]
21. Lee, Q.Y.; Li, H. Photocatalytic Degradation of Plastic Waste: A Mini Review. *Micromachines* **2021**, *12*, 907. [[CrossRef](#)] [[PubMed](#)]
22. Zhao, X.; Lia, Z.; Chen, Y.; Shi, L.; Zhu, Y. Solid-phase photocatalytic degradation of polyethylene plastic under UV and solar light irradiation. *J. Mol. Catal. A Chem.* **2007**, *268*, 101–106. [[CrossRef](#)]
23. Liu, G.L.; Zhu, D.W.; Liao, S.J.; Ren, L.Y.; Cui, J.Z.; Zhou, W.B. Solid-phase photocatalytic degradation of polyethylene–goethite composite film under UV-light irradiation. *J. Hazard. Mater.* **2009**, *172*, 1424–1429. [[CrossRef](#)] [[PubMed](#)]
24. Grigoriadou, I.; Paraskevopoulos, K.M.; Chrissafis, K.; Pavlidou, E.; Stamkopoulos, T.-G.; Bikiaris, D. Effect of different nanoparticles on HDPE UV stability. *Polym. Degrad. Stab.* **2011**, *96*, 151–163. [[CrossRef](#)]
25. Magalhães, F.; Lago, R.M. Floating photocatalysts based on TiO₂ grafted on expanded polystyrene beads for the solar degradation of dyes. *Sol. Energy* **2009**, *83*, 1521–1526. [[CrossRef](#)]
26. Baiocchi, C.; Brussino, M.C.; Pramauroa, E.; Prevot, A.B.; Palmisano, L.; Marci, G. Characterization of methyl orange and its photocatalytic degradation products by HPLC/UV–VIS diode array and atmospheric pressure ionization quadrupole ion trap mass spectrometry. *Int. J. Mass Spectrom.* **2002**, *214*, 247–256. [[CrossRef](#)]
27. Dai, K.; Chen, H.; Peng, T.; Ke, D.; Yi, H. Photocatalytic degradation of methyl orange in aqueous suspension of mesoporous titania nanoparticles. *Chemosphere* **2007**, *69*, 1361–1367. [[CrossRef](#)]
28. Galindo, C.; Jacques, P.; Kalt, A. Photodegradation of the aminoazobenzene acid orange 52 by three advanced oxidation processes: UV/H₂O₂, UV/TiO₂ and VIS/TiO₂. *J. Photochem. Photobiol. A Chem.* **2000**, *130*, 35–47. [[CrossRef](#)]
29. Xu, S.; Zhu, Y.; Jiang, L.; Dan, Y. Visible Light Induced Photocatalytic Degradation of Methyl Orange by Polythiophene/TiO₂ Composite Particles. *Water Air Soil Pollut.* **2010**, *213*, 151–159. [[CrossRef](#)]
30. Li, Y.; Li, X.; Li, J.; Yin, J. Photocatalytic degradation of methyl orange in a sparged tube reactor with TiO₂-coated activated carbon composites. *Catal. Commun.* **2005**, *6*, 650–655. [[CrossRef](#)]
31. Rashed, M.N.; El-Amin, A.A. Photocatalytic degradation of methyl orange in aqueous TiO₂ under different solar irradiation sources. *Int. J. Phys. Sci.* **2007**, *2*, 073–081.
32. Li, Y.; Zhao, H.; Yang, M. TiO₂ nanoparticles supported on PMMA nanofibers for photocatalytic degradation of methyl orange. *J. Colloid Interface Sci.* **2017**, *508*, 500–507. [[CrossRef](#)]
33. XuRauf, M.A.; Ashraf, S.S. Fundamental principles and application of heterogeneous photocatalytic degradation of dyes in solution. *Chem. Eng. J.* **2009**, *151*, 10–18. [[CrossRef](#)]
34. Al-Mamun, R.; Hossain, K.T.; Mondal, S.; Khatun, M.A.; Islam, S.; Khan, Z.H. Synthesis, characterization, and photocatalytic performance of methyl orange in aqueous TiO₂ suspension under UV and solar light irradiation. *S. Afr. J. Chem. Eng.* **2022**, *40*, 113–125. [[CrossRef](#)]
35. Iqbal, A.; Saidu, U.; Adam, F.; Sreekantan, S.; Yahaya, N.; Ahmad, M.N.; Ramalingam, R.J.; Wilson, L.D. Floating ZnO QDs-Modified TiO₂/LLDPE Hybrid Polymer Film for the Effective Photodegradation of Tetracycline under Fluorescent Light Irradiation: Synthesis and Characterisation photodegradation of tetracycline (TC) antibiotics. *Molecules* **2021**, *26*, 2509. [[CrossRef](#)]

Disclaimer/Publisher’s Note: The statements, opinions and data contained in all publications are solely those of the individual author(s) and contributor(s) and not of MDPI and/or the editor(s). MDPI and/or the editor(s) disclaim responsibility for any injury to people or property resulting from any ideas, methods, instructions or products referred to in the content.